Available online at www.sciencedirect.com
SCIENCE DIRECT®
Journal of Molecular Catalysis A: Chemical 223 (2004) 21–29
JOURNAL OF MOLECULAR CATALYSIS A: CHEMICAL
www.elsevier.com/locate/molcata

Redox properties of bis(8-hydroxyquinoline)manganese(II) encapsulated in various zeolites

R. Ganesan, B. Viswanathan*

Department of Chemistry, Indian Institute of Technology, Madras, Chennai 600036, India

Received 12 June 2003; received in revised form 1 March 2004; accepted 5 March 2004
Available online 27 September 2004

Abstract

Bis(8-hydroxyquinoline)manganese(II) [$Mn(C_9H_6NO)_2$ (Mn–Qn)] was encapsulated in NaY, KL, MCM-41, Naβ and Na-ZSM-5. Characterization of the catalysts was done by using IR, UV–vis and EPR spectroscopy whereas redox properties of neat and encapsulated Mn–Qn complexes were evaluated by cyclic voltammetry. Peak broadening and different electrochemical responses are observed upon encapsulation of Mn–Qn complex in various zeolites, thus indicating that Mn–Qn complexes have altered values of redox potential in various positions of zeolite. In order to compare biological systems with metal complexes encapsulated in various zeolites, cytochrome-*c* was immobilized in MCM-41. Redox potential of cytochrome-*c* is shifted towards more positive value upon immobilization in MCM-41. This has been attributed to be due to conformational change of cytochrome-*c* in MCM-41. Change of redox potential of Mn–Qn complex in zeolites is due to change in the positions of HOMO and LUMO levels of metal complexes. Density functional theory (DFT) is employed to calculate the position of HOMO and LUMO levels of metal complexes in zeolite cluster models. The catalytic activity towards oxidation of cyclohexanol was performed using neat and encapsulated Mn–Qn complexes. Encapsulated complexes shows higher activity compared to that of neat complex.

Keywords: Encapsulation; Zeozymes; Cytochrome-*c*; DFT; Cyclohexanol oxidation

1. Introduction

Studies on various complex molecules encaged inside zeolite lattice have attracted attention recently. These zeolite-encaged metal complexes are of importance as catalysts. Each catalytic center is separated in these materials and thereby stability of the complex is also enhanced. Zeolite cages protect the molecule from the decomposition and irreversible dimerization by providing the steric constraints around the molecule [1–19]. Due to these features the zeolite-encaged metal complexes resemble to an extent the enzymes, where the catalytic center might be a transition metal ion and the protein provides the stability and steric constraints. In both systems the complexes of transition metal ion can catalyze the process of oxygen transfer for mild oxidations. Enzymes are capable of carrying out various redox reactions in regio- and sterio-selective manner. Selectivity is imposed in such a natural system by virtue of alteration of the redox potential of metal complexes due to encapsulation in various protein mantles [20]. By adjusting the redox potential of metal complexes, enzymes catalyze various reactions in a highly specific manner. As in the biological systems, one can alter the redox potential of metal complexes by encapsulating them in the zeolites (Fig. 1) [21]. From the knowledge of the redox potential of metal complexes in various zeolites, one can selectively choose a suitable system for a particular reaction. Inorganic complexes encapsulated in such porous systems have therefore been termed as zeozymes. The reasons for the alteration of redox potential of metal complexes in zeolites and biological systems are not clearly stated in the literature [22]. In the present investigation, attempts are made to correlate the redox potential of metal complexes encapsulated in various zeolites with physical

* Corresponding author. Tel.: +91 44 257 8250; fax: +91 44 235 0509.
E-mail address: bvnathan@iitm.ac.in (B. Viswanathan).

1381-1169/$ – see front matter © 2004 Elsevier B.V. All rights reserved.
doi:10.1016/j.molcata.2004.03.055

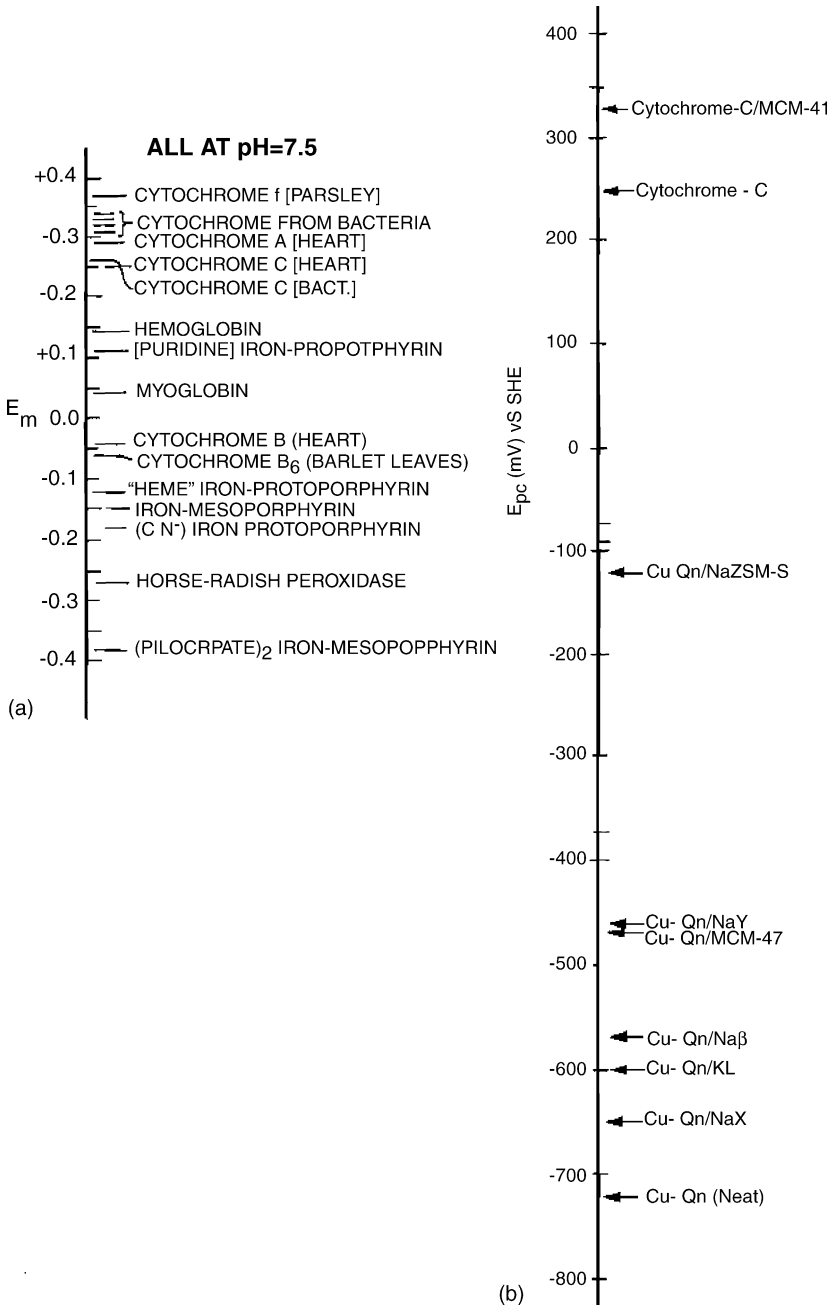

Fig. 1. (a) Redox potentials of various cytochromes, (b) Redox potentials of Cu-8 hydroxy quninoline (Cu–Qn) complexes encapsulated in various zeolites.

properties of zeolites. For this purpose, encapsulation of bis(8-hydroxyquinoline)manganese(II) $Mn(C_9H_6NO)_2$ (Mn–Qn) was carried out in NaY(Si/Al = 2), KL(Si/Al = 3), MCM-41(Si/Al = 30), Naβ(Si/Al = 15) and Na–ZSM-5(Si/Al = 100). The characterization of the catalyst was done by UV–vis, IR, and EPR spectroscopy. The redox properties of metal complexes were studied using cyclic voltammetry, and the results were correlated with the physical properties of the zeolite systems. In order to understand the nature of metal complexes at molecular level in various zeolites, theoretical calculations for neat and encapsulated Mn–Qn complexes in 10- and 12-membered ring clusters were carried out using density functional theory (DFT). The prepared catalysts were tested for the liquid phase-oxidation of cyclohexanol.

2. Experimental

2.1. Preparation of the catalysts

Mn–Qn and manganese-exchanged zeolites were prepared according to the method given in the literature [19,23].

Mn–Qn complex was encapsulated in various zeolites by flexible ligand method. In this method, manganese-exchanged zeolites were heated with excess 8-hydroxyquinoline ligand for 24 h at 393 K in argon atmosphere. The resulting materials were Soxhlet-extracted in acetone to remove the excess ligand as well as complex present on the external surface. Cytochrome-*c* was immobilized by adding 5 ml of 150 μM cytochrome-*c* solution in phosphate buffer (pH = 6.0) to 100 mg of MCM-41. The mixture was then stirred for 2 h in an ice bath [24]. The supernatant liquid was separated from the solid material by centrifugation. The amount of immobilized enzyme was calculated from the difference in absorbance of supernatant liquid at 409.6 nm before and after addition of the support. The cytochrome-*c* immobilized in MCM-41 was washed with de-ionized water and air-dried.

2.2. Characterization of the catalysts

Mn(II) content was estimated according to method reported by Vogel [25]. UV–vis spectra were recorded with Lambda 17 spectrometer. For neat complex the spectra were recorded in DMSO using 1 cm quartz cell, whereas for encapsulated system, the spectra were recorded in Nujol mode at room temperature. The IR spectra were recorded in the range 4000–400 cm^{-1} at room temperature using KBr-diluted pellet. EPR spectra were recorded at liquid nitrogen temperature. The cyclic voltammograms of neat and encapsulated complexes were recorded on a Wenking potentioscan POS73 with digital 2000 X-Y, recorder and 0.1 M KCl was used as supporting electrolyte. The working electrode was prepared by taking 1:1 weight ratio of neat or encapsulated metal complexes and vulcanXC-72 carbon and dispersed in 1 ml of water. This suspension was ultrasonicated for 15 min. Ten microliter of this dispersion was coated on glassy carbon, and 5 μL of 5% nafion (binder) is added on these coatings and dried. This glassy carbon was used as working electrode. Platinum foil was used as counter electrode and Ag/AgCl as reference electrode. The cyclic voltammogram of neat complex was also taken in solution mode by dissolving 0.01 M of Mn–Qn in DMSO using 0.1 M tetra butyl ammonium perchlorate as supporting electrolyte. Platinum foil was used as working electrode.

2.3. Catalytic activity

Liquid-phase oxidation of cyclohexanol was carried out in a glass reactor (50 mL). The reactor was equipped with reflux condenser. In a typical experiment, 100 mg of the desired catalysts was introduced in to the flask and 1:1 mole ratio of cyclohexanol and 30% hydrogen peroxide was added and stirred for 24 h. At the end, the reaction mixture was centrifuged and the products were analyzed in a gas chromatograph (Nucon) equipped with FID and OV 17 column.

3. Computational details

The DFT calculations reported in this article were carried out using the Gaussian 98 program. All DFT calculations were done by Becke three parameter hybrids functional with the LYP correlation function (B3LYP) [26] and an effective core potential basis set LanL2DZ [27]. Clusters of 10 ($Si_{10}O_{10}H_{20}$)(D_{10}h symmetry)- and 12 ($Si_{12}O_{12}H_{24}$)(D_{12}h symmetry)-membered ring systems with 40 and 48 atoms, respectively, were used for the simulations, where the residual valence of silicon atoms were saturated with hydrogen atoms. The optimization of geometry was obtained by using universal force field approach (UFF1.02). In a typical calculation method, the Mn–Qn complex was placed at the center of 10 (Si_{10})- and 12 (Si_{12})- membered ring systems and geometry was optimized by universal force field approach. Advantages of UFF [28] include the fact that it uses a 'first-principles approach', where the atomic parameters are based only on the element, its hybridization and its connectivity. Another advantage is that UFF includes metallic elements such as copper, allowing modeling of metal complexes. In addition to the fact, that UFF is free from molecule-specific. Cerius2 software was used for force field calculations. Using force field-optimized parameters, DFT calculations were done at B3LYP/LanL2DZ level. Similar procedure was used to obtain force field-optimized geometries with different heteroatom (B, Al, Ga)-substituted clusters.

4. Results and discussion

4.1. Elemental analyses

The amount of metal complexes present in both neat and encapsulated complexes are given in Table 1. The metal content, which is obtained for neat complex (16.06%), is matching well with reported value in the literature (16.03%) [23]. Elemental analyses prove that neat complex has metal to ligand ratio of 1:2. In the case of cytochrome-*c*, change in absorbance is measured before and after addition of the support. The amount of cytochrome-*c* immobilized on MCM-41 materials is found to be 1.2×10^{17} molecules/g of MCM-41.

4.2. Infrared spectroscopy

The infrared spectrum of neat complex shows major bands between 1300–1600 cm^{-1}, which correspond to C=C and

Table 1
Elemental analysis for neat and encapsulated Mn–Qn complexes

Catalyst	Wt.% of Mn (II)	No of moles of Mn–Qn/g
Mn–Qn	16.06 (16.03)	
Mn–Qn–NaY	3.5	6.37×10^{-4}
Mn–Qn–KL	2.9	5.28×10^{-4}
Mn–Qn–MCM-41	2.09	3.8×10^{-4}
Mn–Qn–Na–ZSM-5	1.49	2.71×10^{-4}

Table 2
IR, UV–vis spectral data for neat and encapsulated Mn–Qn complexes

Catalyst	ν_1 (cm^{-1})	ν_2 (cm^{-1})	ν_3 (cm^{-1})	ν_4 (cm^{-1})	λ_{max} (nm)
Mn–Qn–Neat	1497.6	1462.4	1382.4	1318.4	396
Mn–Qn–NaY	1497.6	1462.4	1382.4	1318.4	388.2
Mn–Qn–KL	1494.0	1459.2	1382.4	1318.4	393.6
Mn–Qn–Naβ	1499.0	1457.0	1423.0	1380.4	365.0
Mn–Qn–MCM-41	1494.0	1462.4	1379.2	1312.0	364.0
Mn–Qn–NaZSM-5	1472.0	1404.0	1369.0	1369.0	308.4

C=N stretching frequencies of 8-hydroxy quinoline ligand [29]. Upon encapsulation in various zeolites similar type of bands are observed (Table 2). It indicates that same metal complex is present inside the zeolite matrix. In the case of MCM-41 and ZSM-5 IR bands are shifted towards lower frequency, which may be due to the interaction of metal complex with zeolite matrix.

4.3. UV-vis spectroscopy

The UV–vis spectra of neat Mn–Qn and Mn–Qn–NaZSM-5 zeolites are depicted in Fig. 2. UV–vis spectrum of neat complex shows major bands at 396 nm which can be assigned to $\pi \rightarrow \pi^*$ transition of metal complexes [30]. Upon encapsulation of Mn–Qn complex in various zeolites, the band position (Table 2) is blue shifted (3–88 nm). The distortion of the metal complex upon encapsulation in various zeolites might change the position of HOMO and LUMO level of metal complexes. This is further supported by theoretical calculations, which shows that the gap between HOMO and LUMO level of Mn–Qn complex increases upon encapsulation in 10- and 12-membered ring systems. In the case of cytochrome-*c*, similar bands are observed before and after immobilization

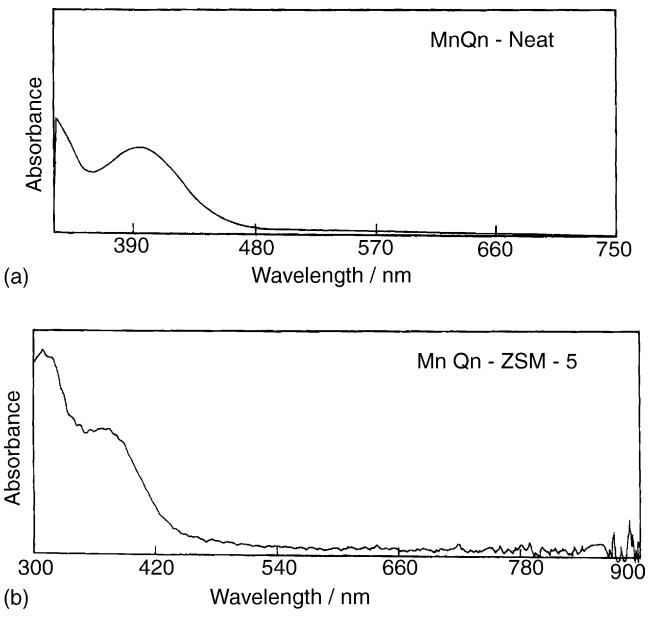

Fig. 2. (a) UV–vis spectra of Mn–Qn in DMSO, (b) Mn–Qn–ZSM-5.

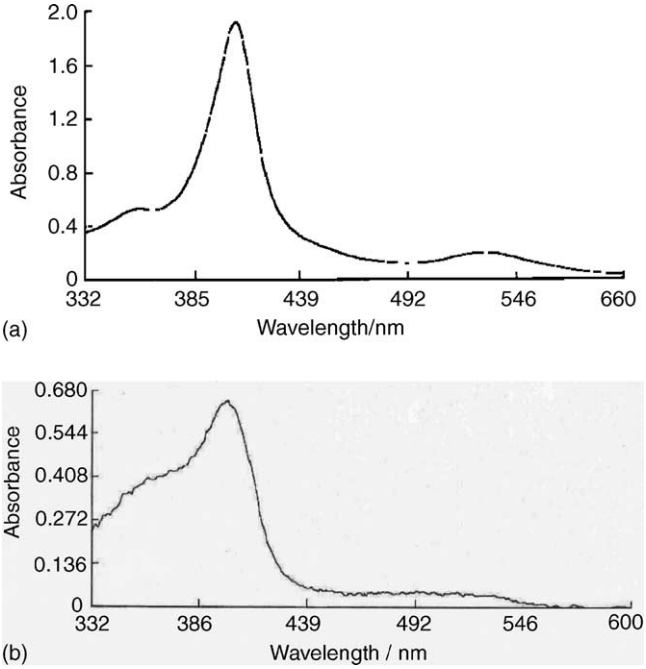

Fig. 3. (a) UV–vis spectra of cytochrome-*c*, (b) cytochrome-*c*-MCM-41.

of cytochrome-*c* on MCM-41 (Fig. 3). It suggests that cytochrome-*c* is immobilized on mesoporous materials.

4.4. EPR spectroscopy

The EPR spectrum of neat complex in solid state shows a broad line and is not resolved even at liquid nitrogen temperature (Fig. 4a). The local magnetic field produced by an electron at a distance *r* (cm) is given by

$$H = \frac{3\beta_e}{r^3}$$

Then even at a distance of 4 Å the local field is about 600 gauss. This large local field will affect neighbouring electron spins, alters the field there and cause a precessing of magnetic dipoles. This interaction causes the lifetime of the excited state to be reduced and hence broadens the line. In frozen DMSO solution it shows a sextet pattern (Fig. 4b), which matches well with the expected spectrum. In the presence of DMSO the active species are diluted and it will reduce the dipolar interactions. Solvation in the axial position is enough to alter the energy levels as well as the zero field splitting to get well-resolved spectrum [31]. The observed *g* value (1.998) and *A* value (96 gauss) for neat complex in DMSO is characteristic of manganese(II) ion (d^5) in octahedral environment [32] with slight distortion in the axial position (Table 3).

Manganese complex present in NaY zeolite shows an isotropic signal. This may be due to higher intermolecular interactions of metal complex inside the zeolite matrix. The EPR pattern of manganese complex is encapsulated in other

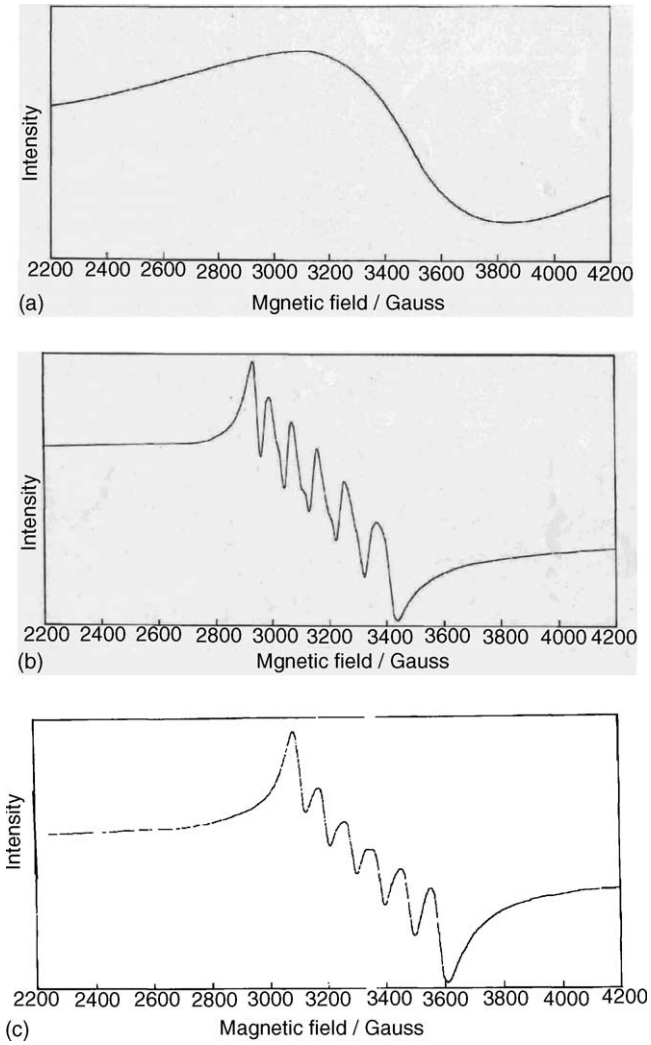

Fig. 4. EPR spectrum of (a) Mn–Qn (solid), (b) Mn–Qn in DMSO, (c) Mn–Qn–MCM-41.

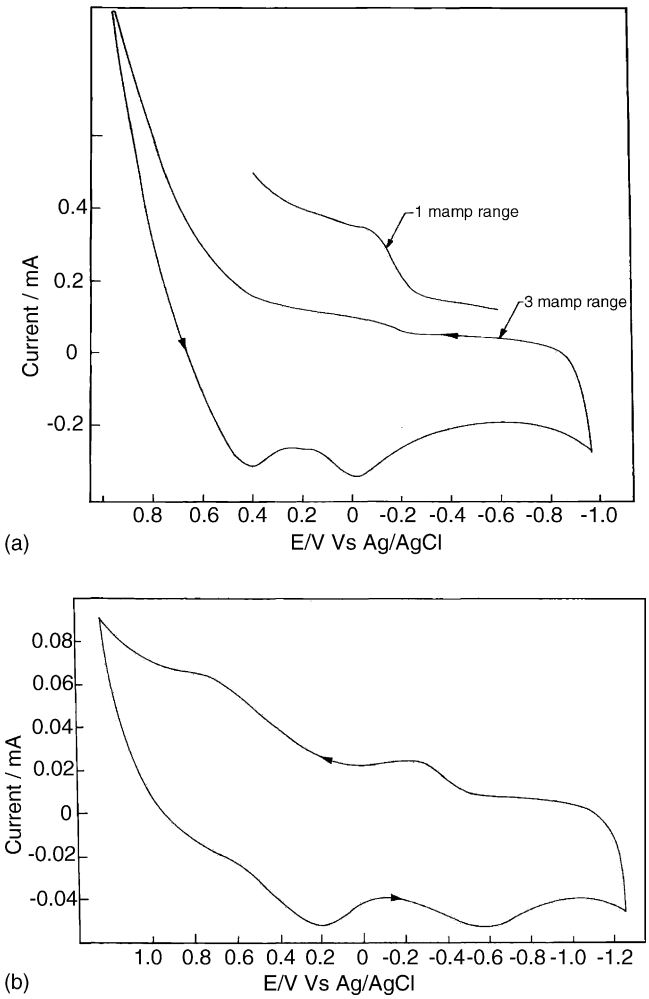

Fig. 5. (a) Cyclic voltammaogram of Mn–Qn in DMSO, (b) Mn–Qn–KL.

zeolites is similar to that of manganese complex in DMSO solvent. (Fig. 4c). This suggests that the manganese complex is present as monomer in various zeolites and axially coordinated with zeolite hydroxyl groups. The differences observed in g_{av} and A_{av} values between neat and manganese complex present in various zeolites are due to axial distortion of manganese complex in various zeolites.

Table 3
EPR spectral parameters for neat and encapsulated Mn–Qn complexes

Catalyst	g_{av}	A_{av}
Mn–Qn (solid)		
Mn–Qn (DMSO)	1.998	90
Mn–Qn–NaY	2.010	NR
Mn–Qn–KL	1.995	96
Mn–Qn–Naβ	2.003	98
Mn–Qn–NaZSM-5	2.020	92
Mn–Qn–NaMCM-41	2.018	94

4.5. Cyclic voltammetry

Fig. 5 shows the cyclic voltammogram of the Mn–Qn and Mn–Qn–KL complex in the potential ranging from −1 to +1 V. The voltammogram of neat complex in solid mode undergoes redox process ($MnQn_2^{2+}/MnQn_2^{3+}$) observed at E_{pc} of −20 mV and E_{pa} of −100 mV (Table 4). The peak separation and I_{pc}/I_{pa} ratio shows that process is quasi-reversible

Table 4
Electrochemical data for neat and encapsulated Mn–Qn complexes

Catalyst	E_{pa}	E_{pc}
Mn–Qn (solid)	−100	−20
Mn–Qn (DMSO)	200	50
Mn–Qn–NaY	500	290
Mn–Qn–KL	690	210
Mn–Qn–Naβ	320	100
Mn–Qn–NaZSM-5	480	450
Mn–Qn–NaMCM-41	410	140
Cytochrome-C	93	26
Cytochrome-C/MCM-41	150	110
Cytochrome-C/MCM-48	170	130

in nature, but in DMSO, this peak is shifted towards more positive value (Table 4) [23]. This is attributed to the solvent coordination in axial position. Neat complex in solution and solid mode shows additional peaks at 0.7 and −0.3 V. It is reported in the literature [23] that most of the oxidized species of Mn–Qn complex undergo dimerization in this potential range. The peak observed at 0.7 and −0.3 V are due to the redox process of dimer. Upon encapsulation in various zeolites, peak broadening is observed, indicating zeolite encapsulated complexes have altered redox potentials in various positions of zeolite matrix. Because of the partial covalent character of the aluminosilicate crystals, electrons are not localized on the framework atoms, rather they are partially delocalized [33]. When a metal complex interacts with an active site, it will perturb all the active sites present within the zeolite so that complex will have different interaction energy and altered redox potential at different places of zeolite. Upon encapsulation in a zeolite matrix, electrochemical behavior of metal complexes arises in different potential ranges. Similar types of observations are made for cobalt salen, ruthenium bipyridyl and iron bipyridyl complexes [34–37]. This may be related to metal complex located at different environments of zeolites. Charge distribution along the framework owing to the partial ionic character of the aluminosilicate crystal generates a strong columbic field inside the cavities, which might activate the metal complex [38]. Because of the zeolite geometry, cages, channels, side packets and charge distribution, field gradients exist [39]. This may alter the energy levels of the metal complex so that metal complexes present at different locations of zeolite have altered redox potentials. As in the biological enzymes, redox potential of same Mn–Qn complex is shifted when it is encapsulated in different zeolites. Redox potential is altered both in biological systems as well as in zeozymes. In order to compare zeozymes with biological systems, cytochrome-*c* has been immobilized in MCM-41. The electrochemical data for neat and encapsulated cytochrome-*c* are given in Table 4. The redox potential is altered towards more positive value upon encapsulation in MCM-41. This is further supported by the observation in the literature [24] where cytochrome-*c* is immobilized on MCM-48. In the literature this shift is attributed to the conformational change of the protein mantle. These observations can be explained as follows: There are two possible interactions when the cytochrome-*c* is encapsulated in zeolite matrix. The protein mantle can interact with Bronsted acid site of the zeolite matrix, which may alter the geometry of the iron

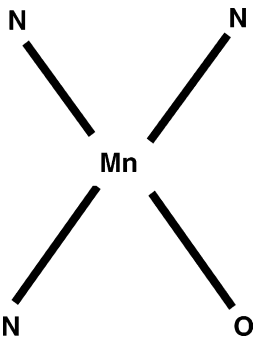

Fig. 6. Representation of the Mn–Qn.

porphyrin active site. Moreover, the axial position of iron porphyrin moiety can also interact with surface hydroxyl groups of zeolite matrix. The net effect leads to the alteration of the redox potential. The redox potential of biological enzyme can also be altered in zeolites as in the metal complexes.

5. Theoretical methods

The redox potential of metal complex is altered in various zeoites due to change in the position of HOMO and LUMO levels of metal complexes. In order to understand the position of HOMO and LUMO levels of metal complexes in various zeolites, theoretical calculations are carried out using density functional theory. The optimized N–Mn and O–Mn bond length and O–Mn–N bond angle (represented in Fig. 6) for neat and encapsulated complexes are given in Table 5. The neat complex is having C_2h symmetry. On encapsulation in 10- and 12-membered ring systems, it deviates from square planarity ($C_2h \rightarrow Ci$ and Cs) (Fig. 7). The bond length between metal and ligand molecule slightly decreases upon encapsulation. Quantum chemical calculations have proven that Si–O bonds in zeolites have a clear covalent character [40]. Valence electrons in zeolites are distributed all over the framework atoms as a partially delocalized electronic cloud. At relatively short distances between the complex molecule and walls of the zeolite cavities, the electron–electron repulsions will be operative [41] because of which the bond length between manganese and ligand molecule decreases.

The HOMO value for neat complex is −7.153 eV and main contribution to HOMO is from p orbital of carbon (98%). Comparison of the energy values of HOMO and LUMO orbital of neat complex with the values obtained in-

Table 5
Force field-optimized parameters of neat and encapsulated Mn–Qn complexes

Catalyst	Mn–O (Å)	Mn–N (Å)	<N_1–Mn–O (deg)	<N_2–Mn–O (deg)
Mn–Qn–Neat	1.963	1.996	94.01	85.99
Mn–Qn–Si_{10}	1.962	1.995	94.08	85.92
Mn–Qn–Si9Al	1.961	1.994	93.94	86.07
Mn–Qn–Si_{12}	1.960	1.994	93.84	86.13
Mn–Qn–$AlSi_{12}$	1.962	1.992	93.83	86.15
Mn–Qn–Al_2Si_{12}	1.961	1.993	93.86	86.14

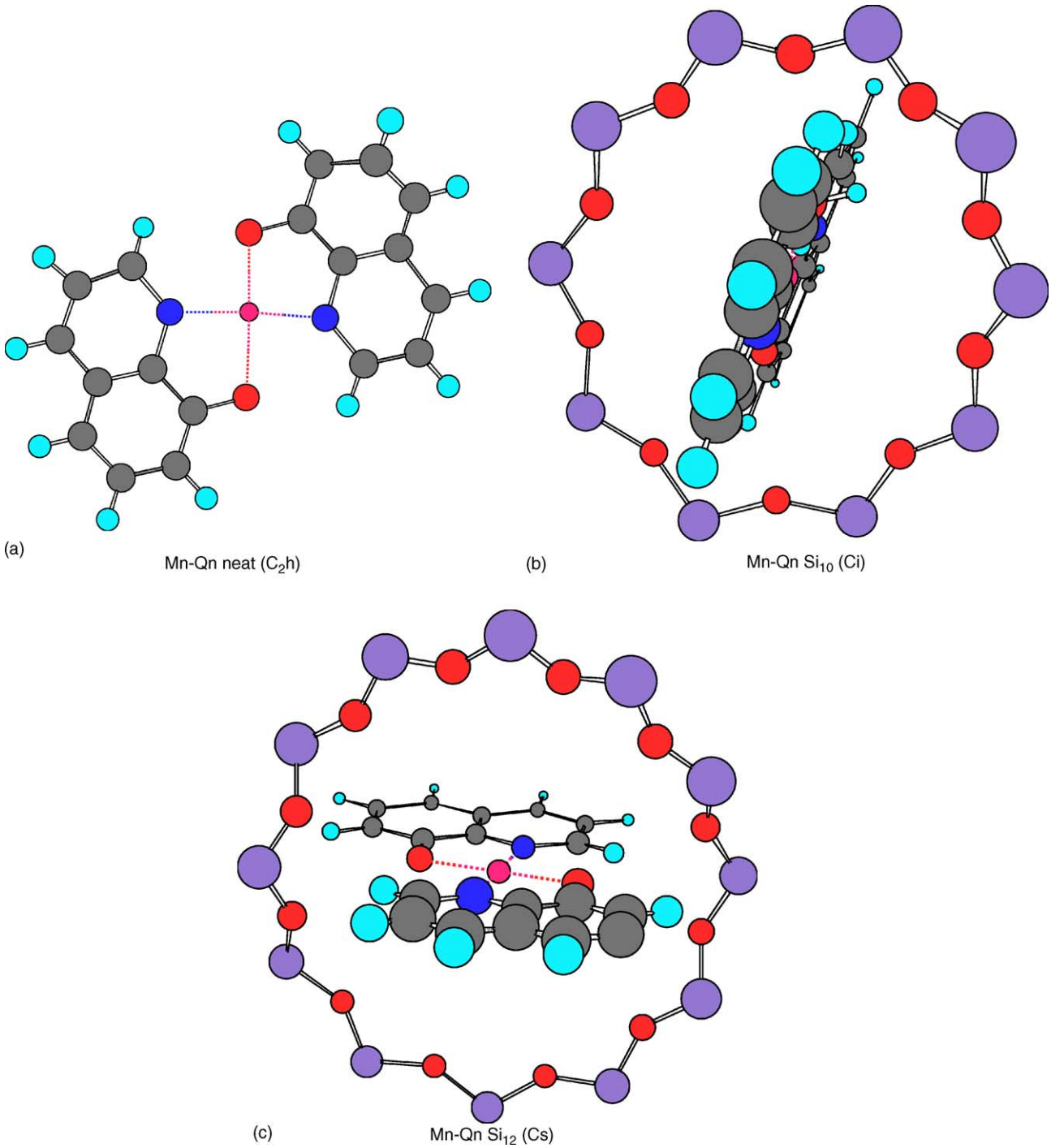

Fig. 7. (a) Mn–Qn model, (b) Mn–Qn–Si_{10}, (c) Mn–Qn–Si_{12}.

side each cluster is given in Table 6. In the case of encapsulated complexes the HOMO and LUMO energy of Mn–Qn is taken from molecular orbitals that have a marked contribution from Mn–Qn molecule. The HOMO of the Mn–Qn in 10-membered ring clusters is stabilized (0.84 eV) more compared to that of Mn–Qn in 12-membered ring systems. This is according to the redox potential measurement where Mn–Qn complex encapsulated in ZSM-5 is shifted more towards positive values compared to NaY.

Table 6
HOMO and LUMO energy levels of neat and encapsulated Mn–Qn complexes

Catalyst	HOMO (eV)	LUMO (eV)
Mn–Qn–Neat	−7.15	−5.93
Mn–Qn–Si_{10}	−7.51	−5.72
Mn–Qn–Si_{12}	−6.67	−5.37
Mn–Qn–$AlSi_{12}$	−6.99	−5.56
Mn–Qn–Al_2Si_{12}	−7.07	−5.66

The type of interaction normally considered when a guest molecule is confined inside the zeolite is due to columbic effects, coordination effects and van der Waals interactions [42]. Columbic effects are produced by the charge distribution along the framework owing to the partial ionic character. This charge distribution generates strong columbic field on the cavities, which might alter the energy level of metal complexes as well as influence the chemical behavior of the transition metal complexes. Coordination effects are produced by Lewis acid–base type interactions among the transition metal complexes and certain sites of the framework in the cavity. Weak electron interactions account for the forces of Van der waals type.

One of the effects that have not been looked in the literature is double layer effect. Zeolite framework is anionic in nature. When the transition metal complex enters the zeolite cavity, it forms a double layer in the zeolite cavities. It is known in the literature that electric field existing in between a double layer is around 10^8 V/cm [43]. This electric field alters the energy levels and chemical behavior of the transition metal complexes. Because of these properties the molecular orbital of metal complex cannot extend over entire space as they are in the neat state but restricted with in the dimension of the zeolite cage. In order to rationalize the influence of aluminum content in the position of HOMO and LUMO levels of metal complexes, replacement of Si → Al, H was done in 12-membered ring systems. The presence of bronsted site changes the electrostatic potential generated inside the cage [44]. In a purely silicious zeolite, negative electrostatic potential, which is acting inside the cavity, creates a given repulsion over the electrons in the complex molecule. This repulsion will increase their energy. If aluminum is introduced, the change O → OH will make the new electrostatic potential less negative due to proton shielding on the corresponding oxygen atom and the electrostatic repulsion over the electron is less. This leads to decrease of energy level of metal complexes. When aluminum is introduced in the zeolites, the HOMO and LUMO level of metal complexes gets stabilized compared to purely silicious zeolites (Table.6).The generation of charge-compensating cation reduces the electric field acting inside the cavity that stabilizes the HOMO and LUMO levels of metal complexes. Since in zeolites aluminum substitution is random one, the molecule, which is present in the sodalite and supercages, cannot experience same electrostatic field. The position of HOMO and LUMO levels of metal complexes will be different in different places of zeolite, which leads to altered redox potential of metal complexes in various positions of zeolites.

6. Catalytic activity

The catalytic activity towards liquid-phase oxidation of cyclohexanol was performed at 308 K using both neat and encapsulated Mn–Qn complexes. The neat complex gives turn-over number of 15. TON increases twenty-seven and thirty-eight times upon encapsulation in NaY and KL zeolites, respectively (Table 7). Selectivity in all cases is 100% for cyclohexanone. The Mn–Qn complex encapsulated in Naβ, NaZSM-5 and Na-MCM-41 zeolites does not show any activity for the oxidation of cyclohexanol. Blank experiments were done in the absence of catalyst and activity was not observed in the absence of catalyst. Of all the catalysts tried, the Mn–Qn complex encapsulated in NaY and KL zeolites only shows catalytic activity and higher turn-over number. This may be due to the alteration of redox potential of metal complexes in various zeolies.

Table 7
Catalytic activity towards oxidation of cyclohexanol by neat and encapsulated Mn–Qn complexes

Catalyst	Conversion to cyclohexanone (mole%)	TON
Mn–Qn	20.0	15
Mn–Qn–NaY	21.4	399
Mn–Qn–KL	23.5	564

Conditions: Weight of the catalyst = 100 mg, Cyclohexanol: H_2O_2 = 1:1, Temperature = 307 K.

7. Conclusions

Mn–Qn complexes are encapsulated in NaY, KI, MCM-41, Naβ and NaZSM-5 zeolites. The differences in band positions of IR, UV–vis and *g* values in EPR between neat and encapsulated complex are attributed to the interaction of metal complex with zeolite matrix. Alterations in redox properties of zeolite-encapsulated complexes can be accounted for on the basis of physical properties of zeolites employed. Theoretical calculations show that the energy values of HOMO and LUMO levels changed upon encapsulation of Mn–Qn complexes. Increasing Al content at the 12-membered ring clusters stabilizes both HOMO and LUMO energy levels of metal complexes. This may be due to decrease of electrostatic field inside the zeolite matrix. The catalytic activity towards oxidation of cyclohexanol was performed using neat and encapsulated encapsulated Mn–Qn complexes. The Mn–Qn complex encapsulated in NaY and KL zeolites are only showing higher activity. All other catalysts are not showing any activity for oxidation of cyclohexanol.

References

[1] B. Viswanathan, J. Energy, Heat, Mass Transfer 8 (1996) 28.
[2] N. Herron, C.A. Tolman, J. Am. Chem. Soc. 109 (1987) 2837.
[3] N. Herron, Inorg. Chem. 25 (1986) 4714.
[4] D.E. Devos, F.T. Starzyk, P.A. Jacobs, Angew. Chem., Int. Ed. Engl. 33 (1994) 431.
[5] D.H. Chatterjee, C. Balaji, A. Das, K. Bhatt, J. Mol. Catal. 92 (1994) 235.
[6] N. Herron, C.A. Tolman, G.D. Stucky, J. Chem. Soc. Chem. Commun. (1986) 1521.
[7] S.H. Law, V. Caps, K.W. Yang, K.Y. Yong, S.C. Tsang, Micro. Meso. Mater. 32 (1999) 279.

[8] C. Baleizao, B. Gigante, M.J. Sabater, H. Garcia, A. Corma, Appl. Catal. A 328 (2002) 279.
[9] A.B. Soorkin, P. Buisson, A.C. Piere, Micro. Meso. Mater. 46 (2001) 87.
[10] D.E. Devos, P.A. Jacobs, Catal. Today 57 (2000) 105.
[11] R.F. Parton, I.V.O.F.J. Vankelecom, M.J.A. Casselman, C.P. Bezoukhanova, J.B. Utterhoven, P.A. Jacobs, Nature 370 (1994) 541.
[12] R. Ganesan, B. Viswanathan, J. Mol. Catal. A 181 (2002) 99.
[13] M.J. Alcon, A. Corma, M. Iglesias, F. Sanchez, J. Mol. Catal. A 144 (1999) 337.
[14] A. Kozlov, A. Kasakura, Y. Iwasawa, J. Mol. Catal. A 137 (1999) 223.
[15] F.T. Starzyk, M.V. Pymbroeck, R.F. Parton, P.A. Jacobs, J. Mol. Catal. A 109 (1996) 75.
[16] S. Ernst, M. Selle, Micro. Meso. Mater. 27 (1999) 355.
[17] C.R. Jacob, S.P. Varkey, P. Ratnasamy, Appl. Catal. A 182 (1999) 91.
[18] X. Hu, K. Meyer, Inorg. Chim. Acta 1 (2000) 1.
[19] C. Bowers, P.K. Dutta, J. Catal. 22 (1970) 271.
[20] W.M. Clark, Oxidation and Reduction Potential of Organic Systems, The Williams and Wilkins Company, Baltimore, USA, 1960.
[21] R. Ganesan, B. Viswanathan, Indian J. Chem. 49A (2001) 255.
[22] E. Briot, V. Bedioui, K. Balkus Jr., J. Electroanal. Chem. 454 (1998) 83.
[23] J.K. Howie, D.T. Sawer, J. Am. Chem. Soc. 98 (1976) 6698.
[24] J.F. Diaz, K. Balkus Jr., J. Mol Catal. B 2 (1996) 115.
[25] A.I. Vogel, Quantitative Inorganic Analysis, Longmans, Green and Co., New York, NY, 1953.
[26] A.D. Becke, J. Chem. Phys. 98 (1993) 5648.
[27] P.J. Hay, W.R. Wadt, J. Chem. Phys. 82 (1985) 270.
[28] A.K. Rappie, C.J. Casewit, K.S. Colwell, W.A. Goodard, W.M. Skiff, J. Am. Chem. Soc. 114 (1992) 10024.
[29] A.K. Nakamoto, Infrared and Raman Spectra of Inorganic Coordination Compounds, Wiley-Interscience Publication, 1975.
[30] L. Morpurgo, R.J.P. Wiiliams, J. Chem. Soc. A 73 (1966).
[31] T.H. Bennur, D. Srinivas, P. Ratnaswamy, Micro. Meso. Mater. 48 (2001) 111.
[32] B.A. Goodman, J.B. Baynor, Adv. Inorg. Chem. Radiochem. 113 (1970) 136.
[33] J. Sauer, Chem. Rev. 89 (1989) 199.
[34] E. Briot, F. Bedioui, K. Balkus Jr., J. Electroanal. Chem. 454 (1998) 83.
[35] F. Bedioui, E.De. Boysson, J. Devynck, K. Balkus Jr., J. Chem. Soc., Faraday Trans. 87 (1991) 3831.
[36] C.A. Bessol, D.R. Rolison, J. Phys. Chem. 101 (1997) 1148.
[37] K. Balkus Jr., A.G. Gabridov, S.T. Bell, F. Bedioui, L. Rowe, J.A. Devynck, Inorg. Chem. 33 (1994) 67.
[38] L. Utterhoven, D. Dompas, W.J. Mortier, J. Chem. Soc., Faraday Trans. 88 (1992) 2753.
[39] G.O.A. Janssens, B.G. Baekelandt, H. Toufar, W.J. Mortier, R.A. Schoonheydt, J. Phys. Chem. 99 (1995) 3251.
[40] E.G. Derouane, J.G. Fripat, J. Phys. Chem. 91 (1987) 145.
[41] A.C. Pullikotil, Ph.D Thesis. I.I.T., Madras, 1995.
[42] C.M.Z. Wilson, A. Corma, P. Viruela, J. Am. Chem. Soc. 98 (1994) 10863.
[43] A.J. Bard, L.R. Faulkner, Electrochemical Methods, Funtamentals and Applications, Wiley, 2000.
[44] A. Corma, H. Garcia, G. Sastre, P. Viruela, J. Phys. Chem. 101 (1997) 4575.